Immobilisation of Zinc porphyrins on mesoporous SBA-15: Effect of bulky substituents on the surface interaction

Immobilisation of Zinc porphyrins on mesoporous SBA-15: effect of bulky substituents on the surface interaction

Elena Balantseva, Ivana Miletto, Salvatore Coluccia and Gloria Berlier*

Università di Torino, Dipartimento di Chimica and NIS Centre of Excellence, Via P. Giuria 7, 10125 Torino, Italy

*corresponding author: gloria.berlier@unito.it; Phone: 0039 0116707856; Fax: 0039 0116707953

Abstract

Two Zn porphyrin complexes, Zn-5,10,15,20-tetrakis(3,5-di-tert-butylphenyl)porphyrin (ZnTBPP) and Zn-tetraphenylporphyrin (ZnTPP) were prepared and physically adsorbed on the surface of mesoporous SBA-15. The resulting materials were tested about the stability of the adsorbed dyes to leaching, and characterized by X-ray diffraction analysis (XRD), low temperature nitrogen adsorption/desorption isotherms, infrared and electronic (Diffuse Reflectance UV-Visible adsorption and emission) spectroscopies. Thermogravimetric and spectrophotometric analyses indicates a surface concentration around 1/40 molecule/nm^2, on an average. The high dispersion of the complexes within the silica pores was suggested by the negligible modifications of the ordered mesoporous structure and textural properties (specific surface area and porosity). A detailed spectroscopic analysis allowed investigating the molecular interaction with silica surface, taking place through hydrogen bonding with Si-OH groups. In the case of ZnTBPP this interaction was mediated by the bulky *tert*-butyl substituents. This resulted in a higher stability to leaching and in a consistent blue-shift of the adsorption and emission bands typical of porphyrins, suggesting a more efficient orbital overlapping between porphyrin and phenyl groups as a result of hindered rotation. This effect was less evident in the ZnTPP complex, which was shown to directly interact with surface Si-OH through the aromatic rings.

Keywords

Zinc porphyrin, SBA-15, infrared, UV-Vis, luminescence, photodynamic therapy

1. Introduction

The chemistry of porphyrins has a long and fruitful history and in present days involves a variety of practical areas, such as medicine, textile industry, chemical analysis and catalysis [1-3]. Among the others, photodynamic therapy (PDT) for cancer treatment and the exploitation of alternative energy sources are the most promising applications [4-10]. For both applications, the key role of porphyrins is the harvesting of light and in its effective conversion and transfer. In this view, one of the main issues is the improvement of light conversion efficiency, which could be dramatically decreased as an effect of molecular association [11-14].

An important aspect influencing the efficiency of PDT process is related to the transport of the photoactive molecule to the desired target, without affecting its structural integrity. Both aspects could be solved by employing appropriate carriers, which are able to bind and transport the bio-agent, concomitantly preventing the molecules association through encapsulation or dispersion on the matrix surface. Promising results in this field were reported, involving silica based materials for porphyrins immobilization or covalent linking [15-20]. Among the others, mesoporous silica materials (particularly in the form of nanoparticles) are regarded as a new frontier in nanomedicine, for the versatility of the carrier that can be easily functionalised with different molecules or "supermolecules" [21, 22].

Mesoporous silica (MPS) materials were firstly proposed at the beginning of the nineties [23, 24], and their success as matrices or carriers for many applications is related to a huge surface area, large pore size and pore volume. No less important is the fact that silica-based structures have good biocompatibility, high tolerance to many organic solvents [25, 26] and easy surface functionalisation [27]. Among the different applications we quote catalysis [17, 28], drug delivery [27, 29-32], cell labelling [33-35], optical sensing [36, 37], biomolecules immobilisation [38-40], and photostabilisation of antioxidants [41-43]. Furthermore, the surface of MPS structures can be easily functionalised for

targeting tumour cells specifically in vivo. These aspects, together with the potential to circumvent drawbacks of photosensitizer delivery systems, makes them attractive as carriers for PDT applications [44].

SBA-15 mesoporous silica was selected to immobilize porphyrin dyes, thanks to the large size of ordered pores (up to 10 nm) [45, 46], that can host bulk molecules such as substituted porphyrins, at the same time providing access to oxygen molecules from the external environment. Despite these peculiarities and several reports about the employ of SBA-15 for drug immobilization[38], only few examples were devoted to SBA-15/porphyrin systems [47]. For instance, meso-meta-tetra(hydroxyphenyl)chlorine (m-THPC) was incorporated into silica by non covalent encapsulation, showing a good spectral correspondence between free and embedded m-THPC and an increase of singlet oxygen $^1O_2$ production with respect to free porphyrin.

Different methods can be employed to prepare hybrid materials based on the incorporation/immobilisation of drugs/photoactive molecules in inorganic, silica-based, materials. These include methods for non covalent [38, 48] or covalent incorporation [15, 49, 50], depending on the materials and applications. As for the non covalent interaction, usually adsorption from solution or incipient wetness impregnation are employed, with variations including heating of a powder mixing of the two components [38], or the “kneading” method, which employs a very small amount of acetone solution [43]. Other approaches include one-pot synthesis methods, to obtain the encapsulation of the photosensitizer within porous nanoparticles [48], silica [47] or organically modified silica (ORMOSIL) particles [51, 52], both allowing gradual release and contact with oxygen of the dye.

Notwithstanding the large variety of available porphyrin structures, only few (including Protoporphyrin IX, the classical structure for PDT) were employed in inclusion complexes [52]. Recent results showed the important role of bulk substitutes of porphyrins on their electronic properties when adsorbed on surfaces [7, 9, 53-55]. Accordingly, two similar metal porphyrin structures were selected

for this work, Zn-5,10,15,20-tetrakis(3,5-di-*tert*-butylphenyl)porphyrin (ZnTBPP) and Zn-tetraphenylporphyrin (ZnTPP) (Scheme 1). In the former, the presence of 3,5-di-*tert*-butylphenyl substitutes promotes a higher solubility, while preventing dye molecules agglomeration and dimer formation, which would result in a decrease of their chromophore activity [56-58]. Thus, SBA-15 was employed to encapsulate ZnTPP and ZnTBPP complexes within the porous structure by adsorption from solutions. The resulting hybrid materials were characterized to obtain information on the effective porphyrin immobilisation by powder X-ray diffraction (XRD), thermogravimetric and gasvolumetric analyses. The interaction of the molecules with the silica surface was investigated by Fourier Transform infrared (FTIR) and electronic spectroscopies, the latter both in adsorption (Diffuse reflectance, DR UV-Vis and luminescence). Comparison of the data obtained on the two complexes on silica and in solution allowed us to evaluate the effect of the bulky substituents on the interaction with the surface.

2 Experimental

2.1 Materials

2.1.1 Synthesis of SBA-15

Ordered mesoporous SBA-15 silica was prepared according to the literature[45]. Briefly, triblock copolymer Pluronic P123 was dissolved in water, a 2 M HCl solution was added and the suspension was kept under stirring at 40 °C for 2 hours. Afterwards, tetraethyl orthosilicate (TEOS) was added drop wise, under continuous stirring. All reagents and solvents were purchased by Sigma-Aldrich and used as received. After 24 h, the silica suspension was transferred into a Teflon lined autoclave and placed in an oven for hydrothermal treatment at a temperature of 90°C for 48 h. The

formed precipitate was filtered off and washed with abundant demineralised water, then the triblock copolymer was removed from the as-prepared material through calcination at 550°C, under N_2 and subsequent O_2 flux.

Tetraphenylporphyrin (TPP) was synthesized and purified as reported in Ref. [59], while for the 5,10,15,20-tetrakis(3,5-di-*tert*-butylphenyl)porphyrin (TBPP) the method proposed in Ref. [60] was followed. The corresponding Zn-porphyrin complexes (ZnP) were prepared by mixing a $2.0 \cdot 10^{-4}$ M benzene solution of the porphyrin ligand with the same concentration of Zinc acetate in methanol [61]. The resulting solution was refluxed for 1 hour until the bands due to the free ligand disappeared in the UV spectrum. It was then washed with distilled water, concentrated, and purified by column chromatography on Al_2O_3. The final product was recrystallized by methanol.

2.1.2 Preparation of porphyrin/silica hybrid materials

ZnP/SBA-15 materials were prepared by adsorption from solution, by quickly adding weighted SBA-15 aliquots, previously treated at 300 °C in vacuum to remove adsorbed water, to ZnP solutions. Different solvents were employed, depending on ZnP solubility: ZnTBPP was dissolved in cyclohexane and ZnTPP in chloroform. In both cases 200 mg of outgassed SBA-15 were added to 40 ml of $2.1 \cdot 10^{-4}$ M ZnP solutions. All suspensions were stirred at room temperature (RT) for 30 minutes. The resulting materials were recovered by centrifugation (10 minutes at 6000 rpm) and dried in air at 40°C.

Supernatant analysis was carried out to estimate ZnP uptake from SBA-15 silica and to study their leaching upon repeated washing with the corresponding solvents (cyclohexane/chloroform). To this aim, a Cary 300 UV-Vis Spectrophotometer (Varian) was employed, working at λ= 545 and 552 nm for ZnTBPP and ZnTPP, respectively. Calibration curves were obtained with diluted solutions over

the range 5.0×10^{-6} - 5.3×10^{-5} M. The molar extinction coefficients (ε) were 2.42×10^{4} and 2.15×10^{4} $M^{-1}\cdot cm^{-1}$ (R^2 = 0.994) for ZnTBPP and ZnTPP, respectively.

2.2 *Characterization*

Powder X-Ray Diffraction (XRD) patterns were obtained with a Philips 1830 instrument, operating with Co Kα radiation, generated at 20 mA and 40 kV. Specific surface area (SSA) and porosity were analyzed by N_2 adsorption-desorption isotherms at liquid nitrogen temperature (LNT) using a Micromeritics ASAP2020 instrument. SSA was calculated by the Brunauer-Emmett-Teller method (BET); pore volume (total and mesopore, the latter in the 50-150 Å range) and average pore size were estimated using the Barrett-Joyner-Helenda method with the Kruk-Jaroniec-Sayari equations (BJH/KJS). Micropore volume was calculated with t-plot method. All calculations were performed on the adsorption branch of the isotherms.

Thermal Gravimetric Analysis (TGA) was carried out on a TAQ600 (TA Instruments) heating the samples at a rate of 10 °C/min from RT to 800 °C in a nitrogen flow. Before starting the measurements, the samples were equilibrated at 30 °C.

Fourier Transform Infrared (FTIR) spectra were collected in transmission mode with a Bruker IFS88 spectrometer equipped with DTGS detector, working at a resolution of 4 cm^{-1}. Self-supporting wafers (ca. 2 mg/cm^2) suitable for transmission measurements were prepared and inserted in quartz cells equipped with KBr windows, allowing in situ activation (room temperature outgassing) before the measurements. Diffuse Reflectance UV-Vis spectra of the powders were collected with a Varian Cary 5000 spectrophotometer equipped with a $BaSO_4$ covered integrating sphere.

Photoemission and excitation steady-state spectra were acquired with a Horiba Jobin Yvon Fluorolog3 TCSPC spectrofluorimeter equipped with a 450 W Xenon lamp and a Hamamatsu R928 photomultiplier. The spectral response was corrected for the spectral sensitivity of the photomultiplier.

Solutions and suspensions were kept in contact with air, because dissolved oxygen was expected to be quite ineffective as quenching agent toward fluorophores with lifetimes shorter than 5 ns, [62] as typically exhibited by porphyrins. Fluorescence lifetimes were measured using a time-correlated single photon counting (TCSPC) technique (Horiba Jobin Yvon) with excitation source NanoLed at 455 nm (Horiba) and impulse repetition rate of 1 MHz at 90° to a TBX-05 detector. The instrument was set in the Reverse TAC mode, where the first detected photon represented the start signal by the time-to-amplitude converter (TAC), and the excitation pulse triggered the stop signal. DAS6 decay analysis software was used for lifetime calculation.

3. Results and Discussion

The inclusion of ZnTBPP and ZnTPP into the pores of SBA-15 was performed by physical adsorption from saturated solutions of ZnP complexes in cyclohexane or chloroform, respectively. The ZnP loading was calculated by spectroscopic analysis by measuring the amount in the supernatant before and after impregnation, and checked by TGA (Table 1). The agreement between the values estimated by the two techniques for each sample is not perfect, but is within the experimental error, considering the low amount. Table 1 also reports the loading expressed as molecule/nm^2, calculated by employing the SSA measured on the parent SBA-15 (see below).

All the following results were obtained on the as-prepared materials, with the loading listed in Table 1. However, spectrophotometric analysis was also carried out to check the leaching of ZnP from the silica matrix, by employing the corresponding solvent (cyclohexane for ZnTBPP and chloroform for ZnTPP) for consecutive washing steps (Figure 1). The results suggest a different stability of the two complexes within SBA-15 pores. While the leaching of ZnTBPP ranges from a 20% loss in the first washing step, up to a final 33% total loss, ZnTPP is easily removed from the matrix in a single washing step (*ca* 72% decrease), but is stable in the consecutive steps. Interestingly, similar experiments

performed in water did not show any appreciable leaching of the ZnP complexes from the matrix, in agreement with the low solubility of the molecules. This suggests that ZnP/SBA-15 could be a stable candidate for use in biological environments.

3.1. Characterization of ZnP/SBA-15 Hybrid Materials.

The dye-silica materials were characterized by XRD and N_2 adsorption-desorption analyses to obtain information on the mesoporous structure before and after immobilisation of Zn-porphyrins and to monitor the effect of ZnP inclusion. Figure 2 shows the XRD profiles of the parent SBA-15 with those of the two ZnP/SBA-15 materials. The diffraction patterns are very similar in all cases and show the (100), (110), and (200) reflections typical of a hexagonal array of pores. This indicates a negligible effect of the dye inclusion on the mesostructure of silica.

The results obtained by gas-volumetric analysis are summarized in Figure 3 and Table 2. The materials show a type IV isotherm, typical of mesoporous materials with one-dimensional cylindrical channels [63, 64]. After impregnation, SSA decreases in a similar way in both inclusion complexes (Table 2). The H1-type hysteresis loop 0.67-0.72 p/p_0 in the SBA-15 isotherm corresponds to N_2 capillary condensation within large mesopores. The same trend is present in the isotherms of dye loaded samples with very small downward shift, corresponding to a decrease in the pore diameter from 99 to 98 Å, irrespective of the molecule. Due to the very small entity of this change (similarly to what observed for pore volumes) it is not possible to safely ascribe it to the presence of ZnP complexes. At pressure above 0.9 p/p_0, another narrow hysteresis loop is observed for all samples, due to nitrogen condensation in textural porosity. On the whole, this analysis indicates a relatively small effect of ZnP inclusion in SBA-15, in agreement with the low loading, suggesting a high dispersion of the complexes within the pores.

3.3. FTIR Spectroscopy

FTIR spectroscopy was employed to confirm the structural integrity of the molecules and to study their interaction with the surface of silica. The results are reported in Fig. 4, together with the spectra of bare SBA-15 and of the two complexes, for comparison. In the high frequency region (top panel of Fig. 4), the spectrum of parent SBA-15 is characterized by a strong and narrow peak at 3742 cm^{-1}, with a weaker component at 3713 cm^{-1} and a broad absorption between 3700 and 3000 cm^{-1} (maximum at 3582 cm^{-1}). These are well known features related to isolated (3742 cm^{-1}), terminal (3713 cm^{-1}) and hydrogen bonded surface Si-OH groups (3700-3000 cm^{-1}) [64-67]. The weak bands at 2926 and 2856 cm^{-1} are due to small amounts of hydrocarbon impurities.

In the same panel the spectra of the two ZnP complexes are shown in the 3200-2700 cm^{-1} range only, since no significant signals are present at higher frequency. ZnTPP (grey curve) shows weak bands above (3054 and 3020 cm^{-1}) and below 3000 cm^{-1} (2920 and 2850 cm^{-1}), which can be assigned to aromatic and aliphatic C-H stretching modes (ν*C*H), respectively, in agreement with what reported for metal-free TPP [68]. The spectrum of ZnTBPP (light grey) shows similar weak bands at 3120, 3066 and 3050 cm^{-1}, due to aromatic ν*C*H, with intense bands at 2960, 2904 and 2862 cm^{-1}, clearly related to the *tert*-butyl groups. In the spectra of the ZnP-SBA-15 complexes the ν*C*H modes of ZnTBPP are clearly discernible, particularly the most intense bands at 2960 and 2862 cm^{-1} (dotted curve), while ZnTPP-SBA-15 shows intense bands in the region of aliphatic ν*C*H (full curve), which could be related to some hydrocarbon impurities. Both samples show a decrease in the intensity of the bands due to isolated and terminal Si-OH groups (3742 and 3713 cm^{-1}), and a corresponding increase in the broad absorption between 3700 and 3000 cm^{-1} These features indicate that the two ZnP complexes interacts *via* hydrogen bonding with surface Si-OH.

Additional information can be obtained by analysis of the low frequency region (bottom panel of Fig. 4). The spectrum of ZnTPP (grey curve) is mainly characterized by the bands related to the ring

modes (νC=C) of the phenyl and porphyrin rings (1592, 1573, 1524, 1500 and 1486 and 1462 cm^{-1}) and to the corresponding CH bending (δC-H) modes (1440, 1385 and 1340 cm^{-1}) [68, 69]. Important differences can be seen by comparison with the spectrum of the *tert*-butyl substituted complex, ZnTBPP (light grey curve). In particular, the bands at 1573, 1486, 1462, 1440, 1385 and 1340 cm^{-1} are affected both in position and intensity, as a consequence of the phenyl rings substitution. The expected bending modes of the *tert*-butyl groups (asymmetric and symmetric δCH_3) are clearly seen at 1475 (δ_{as} CH_3) and 1362 cm^{-1} (δ_s CH_3).

The spectrum of ZnTBPP-SBA-15 (dotted curve) is very similar to that of the corresponding molecule. The main changes can be seen in the relative intensity and position of the CH bending modes (δCH and δCH_3), which are usually not very sensitive to small changes in the molecular environment. This deserves some comments. On the basis of their chemical structure, one would expect a hydrogen bonding interaction between surface Si-OH groups and the phenyl and porphyrin ring -electrons, with a less important role of the *tert*-butyl substituents. However, the infrared evidence suggests a stronger perturbation of the latter, indicating a modification in their geometry and/or bond lengths. The perturbation of the bulky substituents conformation does not however allow for a porphyrin optimal geometry necessary to optimize hydrogen bonding with the surface.

On the contrary, the spectrum of ZnTPP is strongly modified by the interaction with the silica surface, in that the intensity of the main bands at 1592, 1440 and 1340 cm^{-1} decreases, while new broad absorptions at 1532 and 1465 cm^{-1} are observed, in the typical region of aromatic ring vibrations [69], together with other minor changes. These evidences suggest a more important involvement of the aromatic rings in the formation of hydrogen bonding adducts with surface Si-OH.

3.4. UV-VIS spectral analysis

DR UV-Vis and photoluminescence spectra of the prepared hybrid samples and of the corresponding porphyrin solutions were measured and compared in order to evaluate the effect of the immobilisation on the dyes electronic properties, and to disclose possible correlations between the porphyrin molecular structure and the overall performances of the hybrids.

Absorption and emission spectra of ZnTPP and ZnTBPP solutions are shown in Fig. 5A. The UV-Vis absorption spectra of porphyrins exhibit an intense band at about 400 nm (the Soret or B band) and several weaker absorptions (the Q or α bands) at higher wavelengths (in the 450-700 nm range). Both Soret and Q bands are characteristic "fingerprints" of porphyrin adsorption spectra. The Soret band (usually around 420 nm) is related to a highly permitted transition to the second excited state ($S_0 \rightarrow S_2$), while the Q bands (usually near 550 nm) are due to weakly allowed transitions to the first excited state ($S_0 \rightarrow S_1$) and are usually sensitive to the coordination state of the metal ions. In our case the closed-shell metal ion Zn(II) (d^{10}) is characterized by dπ (dxz , dyz) metal-based orbitals relatively low in energy. Hence these have very little effect on the porphyrin π to π* energy gap in the electronic spectra [1]. Variations of the peripheral substituents on the porphyrin ring often cause negligible changes in the absorption features, both in terms of absorption wavelength and intensity.

Absorption spectra of both ZnTPP and its *tert*-butyl substituted analogue ZnTBPP (Figure 5A) are characterized by an intense Soret band centred at 418-420 nm and Q bands of different relative intensities at 546/587 nm in the case of ZnTBPP and at 551/594 nm in the case of ZnTPP. This comparison indicate a small effect of the bulky substituents on the efficiency of π porphyrin- π phenyl and dπ porphyrin-π phenyl orbital overlapping in spite of their steric effect, suggesting a negligible effect in hindering the rotation of the phenyl rings with respect to the porphyrin one [1]. In the case of ZnTBPP an additional band is observed at 620 nm, which could be attributed to a small amount of metal free complex or to some partial oxidation products, such as the *meso*-tetraphenylchlorin, as reported by Rousseau et al. [70].

Photoluminescence spectra of the porphyrin solutions, obtained upon excitation at 418 nm, are reported in Fig. 5B. The emission profile of ZnTPP is characterized by a broad band in the 550-700 nm range, with two maxima at 602 nm and 646 nm having the same intensity; the emission profile of ZnTBPP is similar but blue shifted, with the two components at 588nm and 640 nm, the longer wavelength one being the most intense.

DR UV-Vis spectra of the ZnP-SBA-15 materials were registered and compared to the absorption spectra of the corresponding ZnP solutions; the spectra are reported in Figs. 6A and 6D with a magnification of the Q bands region in Figs. 6B and 6E. The inclusion of ZnTPP in SBA-15 leads to a slight broadening of the Soret band, along with a significant change in the relative intensity of the Soret and Q bands, the former being almost halved with respect to the solution spectrum. Only a moderate red shift (2-5 nm) is observed in the Q bands (Fig. 6B) upon inclusion. Conversely, the effect of inclusion on the absorption spectrum of ZnTBPP is much stronger (Fig. 6D): we assist to a significant broadening of the Soret band, along with a red shift and a huge decrease in its relative intensity with respect to Q bands. Broadening and a significant red shift (12-13 nm) are also observed for the Q bands. This observation indicates that the electronic properties of both complexes are affected by inclusion, particularly in the case of ZnTBPP. We underline the absence on the hybrid sample of the component formerly observed at 620 nm, assigned to ZnTBPP impurities or oxidation products. This is also confirmed by the analysis of the supernatant after washing (not reported), suggesting that ZnTBPP is the main compound loaded on SBA-15.

It has been widely reported in literature that adsorption of organic molecules on oxide surfaces causes strong perturbations of the absorption maxima and the molar absorption coefficients [71, 72]. One of the most common effect is the broadening of the absorption bands, probably related to the interaction of the aromatic π electrons with the oxide surface [71, 73]. We usually assist to a spectral red shift when the excited state of the molecule has and increased permanent dipole or if it is more

polarizable than the ground state and to a spectral blue shift if the reverse is true [74-77]. Thus, a red shift of the Q-bands and a large absorbance decrease and broadening of the Soret band for ZnP-SBA-15 suggest that ZnP molecules are adsorbed onto SBA-15 and that the porphyrin π-electrons interact with the surface hydroxyl groups of SBA-15. Similar spectral changes for porphyrin adsorption on oxide surfaces have been reported for ZnTPP on TiO_2 [78], CoTPP and H_2TPP on TiO_2 [77], and for H_2TPP loaded on MCM-41 [75]. Moreover Nakagaki et al. showed a similar behavior for zeolite-encapsulated metalloporphyrins compared with the free complexes [79].

Different mechanisms were proposed for the absorption spectral shift exhibited by porphyrins in interactions with oxide surfaces; among them, the more credited are the aggregation effect [80, 81], the solvent polarity effect and the conformation change upon adsorption [82], in particular related to the flattening of the meso-substituent with respect to the plane of the porphyrin ring. The spectral shift due to this mechanism depends on the fact that the molecular flattening will extend the π-conjugation of the porphyrin molecule [82-84].

As far as our results are concerned, the aggregation effect can be excluded because it usually induces more severe changes in the spectra with respect to what we observed; the solvent polarity usually induces only small shift and can play a role in our systems as of course the polarity experienced by the ZnP inside the channels of SBA-15 is different from the polarity of the solvent in which the absorption spectra were registered (chloroform for ZnTPP and cyclohexane for ZnTBPP). Although most of the studies about the molecular flattening and conformational changes of porphyrins have been carried out using nanosheets as inorganic support [85], similar effects can be imagined in the case of the interaction of the ZnP with the SBA-15 surface, due to the large size of the ordered pores. The stronger shift of the absorption spectrum exhibited by ZnTBPP-SBA-15 material suggests a different interaction with the SBA-15 surface with respect to unsubstituted ZnTPP, promoted by the *tert*-butyl substituent. We can thus infer that the interaction of ZnTBPP with surface Si-OH *via* the bulky

substituents, as suggested by FTIR spectroscopy, hinders the free rotation of phenyl rings with respect to the porphyrin rings, extending π conjugation. This effect is somewhat similar to what reported by Fiorilli et al., who observed a different solvatochromic effect of the silica surface towards large dyes molecules depending on the flexibility of the anchoring ligand [86].

Photoluminescence properties of the hybrid materials were evaluated and compared to the corresponding porphyrin molecules in solution (Figs. 6C and 6F). The excitation wavelengths were chosen on the basis of the absorption spectra; hence photoluminescence spectra were recorded by exciting the samples at 418, 545 and 560 nm. The shape of the emission profile does not sensibly changes as a function of the excitation wavelength, which only affects the overall emission intensity. For the sake of brevity and comparison only spectra obtained by exciting at 418 nm are displayed.

Similarly to what observed in absorption, photoluminescence features of the ZnTPP-SBA-15 material are not so significantly different from those of the porphyrin solution: we assist to a moderate red shift (more significant for the longer wavelength component of the spectrum) of the band along with a small change in the relative intensities. More severe modifications were found in the case of the *tert*-butyl substituted ZnP. The photoluminescence profile of ZnTBPP solution is characterized by two main components at 588 and 640 nm; in the case of the ZnTBPP/SBA-15 hybrid the whole spectrum is red-shifted and the two main components are characterized by different relative intensities with respect to what evidenced for the solution. The lower energy band is no longer the more intense, and an intermediate weak component arises (637 nm). A red shift indicates that the adsorption of dyes on SBA-15 causes a decrease in the energy transfer between high and low energy levels of ZnTBPP. This could be due to some structural deformations of ZnTBPP, as already discussed, and/or due to the energy transfer from porphyrin to surface. The presence of the weak component at 637 nm can be explained as a splitting of one band (640 nm in solution) into two components (637 and 653 nm). Energy level splitting is often related to the presence of slightly different emitting species; in the case

of our material we can hypothesize the presence of ZnTBPP molecules undergoing different conformational constraint due to different location within the SBA-15 pores.

An assessment of the dye distribution in the ZnTBPP-SBA-15 hybrid was made on the basis of fluorescence lifetime (τ, Table 3). This is defined by the average time the molecules spend in the excited state prior to return to the ground state and it is measured by fitting the emission decay curves with mono-or bi-exponential functions. The corresponding χ^2 value in Table 3 is an indication of the goodness of the fit.

While in the case of ZnTPP-SBA-15 material the decay curves were well fitted by a mono-exponential function, revealing the presence of a single emitting species, the decay curve of the ZnTBPP-SBA-15 hybrid was fitted by a biexponential decay function. This suggests the presence of two different silica microenvironments around the dye molecules and it is in accordance with both the fluorescence spectral data and the observed two-steps leaching of the ZnTBPP from the hybrid system. For both the materials, however, the τ values are longer than those exhibited by the ZnP solution, suggesting that the entrapment of the molecules within the channels of SBA-15 reduces the ZnTBPP intermolecular collisions and the dye-solvent interactions, extending the fluorescence lifetime of the metal porphyrin.

4. Conclusions

Two Zn porphyrin complexes were adsorbed within the channels of mesoporous SBA-15, resulting in hybrid materials that were characterized about their structural and electronic properties. No evident changes about the textural properties of the silica host (porosity and specific surface area) were observed, indicating a good molecular dispersion of the complexes.

Vibrational (FTIR) and electronic spectroscopies (DR UV-Vis and luminescence) testified of the successful incorporation of the dyes, providing useful information on the molecular interaction and on the solvatochromic effect of the host. Namely, FTIR spectroscopy suggested an important role of the bulky *tert*-butyl substituents in mediating the interaction of ZnTBPP with the silica surface, through hydrogen bonding interactions with Si-OH groups. This interaction also affected the stability of the

complex inside the pores, as observed by leaching tests, and the electronic properties with respect to solution. The observed blue shift suggests a more effective electron delocalization between porphyrin and phenyl rings, as a consequence of hindered phenyl rotation.

On the contrary, vibrational analysis of unsubstituted ZnTPP indicates a more direct involvement of the aromatic rings with surface Si-OH, which results in a lower stability towards leaching. Surprisingly, the blue shift of absorption and emission bands with respect to solution is small, suggesting that the interaction does not dramatically influence the π-π overlapping between porphyrin and phenyl rings.

The previous conclusions are in agreement with luminescence lifetime measurements, showing a minor increase for ZnTPP with respect to solution and a more relevant one for ZnTBPP. Moreover, in the latter case two distinct decay profiles were measured, suggesting different local environments of the included complexes.

Acknowledgments

Compagnia di San Paolo and University of Turin are gratefully acknowledged for funding Project ORTO114XNH through "Bando per il finanziamento di progetti di ricerca di Ateneo - anno 2011". This work was supported by the European COST Action MP1202 "Rational design of hybrid organic inorganic interfaces: the next step towards advanced functional materials".

References

[1] I. Beletskaya, V.S. Tyurin, A.Y. Tsivadze, R. Guilard, C. Stern, Chem. Rev. 109 (2009) 1659-1713.

[2] M. Biesaga, K. Pyrzyńska, M. Trojanowicz, Talanta 51 (2000) 209-224.

[3] E. Brulé, Y.R. de Miguel, Org. Biomol. Chem. 4 (2006) 599-609.

[4] E.D. Sternberg, D. Dolphin, C. Bruckner, Tetrahedron 54 (1998) 4151-4202.

[5] M. Kepczynski, M. Dzieciuch, M. Nowakowska, Curr. Pharm. Design 18 (2012) 2607-2621.

[6] L.-L. Li, E.W.-G. Diau, Chem. Soc. Rev. 42 (2013) 291-304.

[7] W.M. Campbell, K.W. Jolley, P. Wagner, K. Wagner, P.J. Walsh, K.C. Gordon, L. Schmidt-Mende, M.K. Nazeeruddin, Q. Wang, M. Gratzel, D.L. Officer, J. Phys. Chem. C 111 (2007) 11760-11762.

[8] A. Hagfeldt, G. Boschloo, L. Sun, L. Kloo, H. Pettersson, Chem. Rev. 110 (2010) 6595-6663.

[9] J. Jasieniak, M. Johnston, E.R. Waclawik, J. Phys. Chem. B 108 (2004) 12962-12971.

[10] C.-W. Lee, H.-P. Lu, C.-M. Lan, Y.-L. Huang, Y.-R. Liang, W.-N. Yen, Y.-C. Liu, Y.-S. Lin, E.W.-G. Diau, C.-Y. Yeh, Chem. Euro J. 15 (2009) 1403-1412.

[11] C. Di Natale, D. Monti, R. Paolesse, Mater. Today 13 (2010) 37-43.

[12] R. Margalit, M. Rotenberg, Biochem. J 219 (1984) 445-450.

[13] R. Margalit, N. Shaklai, S. Cohen, Biochem. J 209 (1983) 547-552.

[14] Z.J. Chen, A. Lohr, C.R. Saha-Moller, F. Würthner, Chem. Soc. Rev. 38 (2009) 564-584.

[15] A. Molinari, A. Maldotti, A. Bratovcic, G. Magnacca, Catal. Today 161 (2011) 64-69.

[16] E. Fagadarcosma, C. Enache, I. Armeanu, D. Dascalu, G. Fagadarcosma, M. Vasile, I. Grozescu, Mater. Res. Bull. 44 (2009) 426-431.

[17] A.R. McDonald, N. Franssen, G.P.M. van Klink, G. van Koten, J. Organomet. Chem. 694 (2009) 2153-2162.

[18] a.K. Rahiman, K. Rajesh, K.S. Bharathi, S. Sreedaran, V. Narayanan, Inorg. Chim. Acta 362 (2009) 1491-1500.

[19] C. Huo, H. Zhang, H. Zhang, H. Zhang, B. Yang, P. Zhang, Y. Wang, Inorg. Chem. 45 (2006) 4735-4742.

[20] H. Zhang, Y. Sun, K. Ye, P. Zhang, Y. Wang, J. Mater. Chem. 15 (2005) 3181.

[21] K.K. Coti, M.E. Belowich, M. Liong, M.W. Ambrogio, Y.A. Lau, H.A. Khatib, J.I. Zink, N.M. Khashab, J.F. Stoddart, Nanoscale 1 (2009) 16-39.

[22] M.W. Ambrogio, C.R. Thomas, Y.-L. Zhao, J.I. Zink, J.F. Stoddartt, Acc. Chem. Res. 44 (2011) 903-913.

[23] T. Cassagneau, G.B. Hix, D.J. Jones, P. Maireles-Torres, M. Rhomari, J. Roziere, J. Mater. Chem. 4 (1994) 189-195.

[24] J.S. Beck, J.C. Vartuli, W.J. Roth, M.E. Leonowicz, C.T. Kresge, K.D. Schmitt, C.T.W. Chu, D.H. Olson, E.W. Sheppard, J.B. McCullen, J.B. Higgins, J.L. Schlenken, J. Am. Chem. Soc. 114 (1992) 10834-10843.

[25] Y. Zhao, X. Sun, G. Zhang, B.G. Trewyn, I.I. Slowing, V.S.-Y. Lin, ACS Nano 5 (2011) 1366-1375.

[26] S.-H. Wu, Y. Hung, C.-Y. Mou, Chem. Commun. 47 (2011) 9972-9985.

[27] M. Vallet-Regi, F. Balas, D. Arcos, Angew. Chem. Int. Edit. 46 (2007) 7548-7558.

[28] S.H. Joo, J.Y. Park, C.-K. Tsung, Y. Yamada, P. Yang, G.A. Somorjai, Nat. Mater. 8 (2009) 126-131.

[29] S. Wang, Microporous Mesoporous Mater. 117 (2009) 1-9.

[30] S. Sortino, J. Mater. Chem. 22 (2012) 301.

[31] S. Song, K. Hidajat, S. Kawi, Langmuir 21 (2005) 9568-9575.

[32] E. Aznar, R. Martinez-Manez, F. Sancenon, Expert Opin. Drug Deliv. 6 (2009) 643-655.

[33] D.-M. Huang, Y. Hung, B.-S. Ko, S.-C. Hsu, W.-H. Chen, C.-L. Chien, C.-P. Tsai, C.-T. Kuo, J.-C. Kang, C.-S. Yang, C.-Y. Mou, Y.-C. Chen, FASEB J. 19 (2005) 2014-2016.

[34] L. Li, C.-K. Tsung, T. Ming, Z. Sun, W. Ni, Q. Shi, G.D. Stucky, J. Wang, Adv. Funct. Mater. 18 (2008) 2956-2962.

[35] E. Gianotti, C.A. Bertolino, C. Benzi, G. Nicotra, G. Caputo, R. Castino, C. Isidoro, S. Coluccia, ACS Appl. Mater. Interfaces 1 (2009) 678-687.

[36] Z. Jin, X.-B. Zhang, D.-X. Xie, Y.-J. Gong, J. Zhang, X. Chen, G.-L. Shen, R.-Q. Yu, Anal. Chem. 82 (2010) 6343-6346.

[37] L.-L. Li, H. Sun, C.-J. Fang, J. Xu, J.-Y. Jin, C.-H. Yan, J. Mater. Chem. 17 (2007) 4492.

[38] R. Mellaerts, J. Jammaer, M. Van Speybroeck, H. Chen, J. Van Humbeeck, P. Augustijns, G. Van den Mooter, J. Martens, Langmuir 24 (2008) 8651-8659.

[39] Y. Wang, F. Caruso, Chem. Mater. 17 (2005) 953-961.

[40] A. Vinu, N. Gokulakrishnan, V.V. Balasubramanian, S. Alam, M.P. Kapoor, K. Ariga, T. Mori, Chem. Euro J. 14 (2008) 11529-11538.

[41] V. Ambrogi, L. Perioli, F. Marmottini, L. Latterini, C. Rossi, U. Costantino, J. Phys. Chem. Solids 68 (2007) 1173-1177.

[42] L. Gastaldi, E. Ugazio, S. Sapino, P. Iliade, I. Miletto, G. Berlier, Phys. Chem. Chem. Phys. 14 (2012) 11318-11326.

[43] G. Berlier, L. Gastaldi, E. Ugazio, I. Miletto, P. Iliade, S. Sapino, J. Colloid Interface Sci. 393 (2013) 109-118.

[44] P. Couleaud, V. Morosini, C. Frochot, S. Richeter, L. Raehm, J.-O. Durand, Nanoscale 2 (2010) 1083-1095.

[45] D.Y. Zhao, Q.S. Huo, J.L. Feng, B.F. Chmelka, G.D. Stucky, J. Am. Chem. Soc. 120 (1998) 6024-6036.

[46] M. Kruk, M. Jaroniec, C.H. Ko, R. Ryoo, Chem. Mater. 12 (2000) 1961-1968.

[47] F. Yan, R. Kopelman, Photochem. Photobiol. 78 (2003) 587-591.

[48] J. Zhou, L. Zhou, C. Dong, Y. Feng, S. Wei, J. Shen, X. Wang, Mater. Lett. 62 (2008) 2910-2913.

[49] A. Gulino, P. Mineo, I. Fragala, J. Phys. Chem. C 111 (2007) 1373-1377.

[50] A. Gulino, P. Mineo, S. Bazzano, D. Vitalini, I. Fragala, Chem. Mater. 17 (2005) 4043-4045.

[51] K.-T. Yong, I. Roy, M.T. Swihart, P.N. Prasad, J. Mater. Chem. 19 (2009) 4655-4672.

[52] A.G.a.S.H. J. Qian, J. Biomed. Opt. 14 (2009).

[53] A. Forneli, M. Planells, M.A. Sarmentero, E. Martinez-Ferrero, B.C. O'Regan, P. Ballester, E. Palomares, J. Mater. Chem. 18 (2008) 1652.

[54] J.K. Park, H.R. Lee, J. Chen, H. Shinokubo, A. Osuka, D. Kim, J. Phys. Chem. C (2008) 16691-16699.

[55] X. Guo, Z. Dong, D. Fujita, Thin Solid Films 516 (2008) 2407-2410.

[56] J.E. Rogers, K.a. Nguyen, D.C. Hufnagle, D.G. McLean, W. Su, K.M. Gossett, A.R. Burke, S.a. Vinogradov, R. Pachter, P.a. Fleitz, J. Phys. Chem. A 107 (2003) 11331-11339.

[57] T. Chaudhuri, D. Goswami, M. Banerjee, Spectroc. Acta Pt. A-Molec. Biomolec. Spectr. 79 (2011) 131-136.

[58] E.V. Antina, E.V. Balantseva, M.B. Berezin, Makroheterocycles 3 (2012) 228-233.

[59] A.S. Semeikin, O.I. Koifman, B.D. Berezin, Chemistry of Heterecyclic Compounds 22 (1986) 629-632.

[60] M.J. Crossley, P. Thordarson, J.P. Bannerman, P.J. Maynard, J. Porphyr. Phthalocyanines 2 (1998) 511-516.

[61] E.V. Balantseva, Antina E.V, B. M.B., Deposited (2003) 23.

[62] J.R. Lackowitz, Principles of Fluorescence Spectroscopy, Springer Publishing, Singapore (2006)

[63] F. Rouquerol, J. Rouquerol, K. Sing, Adsorption by Powders & Porous Solids, Academic Press, (1999)

[64] S.A. Kozlova, S.D. Kirik, Microporous Mesoporous Mater. 133 (2010) 124-133.

[65] A. Zecchina, S. Bordiga, G. Spoto, L. Marchese, G. Petrini, G. Leofanti, M. Padovan, J. Phys. Chem. 96 (1992) 4985-4990.

[66] F. Musso, M. Sodupe, M. Corno, P. Ugliengo, J. Phys. Chem. C 113 (2009) 17876-17884.

[67] I. Braschi, G. Gatti, C. Bisio, G. Berlier, V. Sacchetto, M. Cossi, L. Marchese, J. Phys. Chem. C 116 (2012) 6943-6952.

[68] M.M. El-Nahass, H.M. Zeyada, M.S. Aziz, M.M. Makhlouf, Spectroc. Acta Pt. A-Molec. Biomolec. Spectr. 62 (2005) 11-15.

[69] G. Socrates, Infrared and Raman characteristic group frequencies, John Wiley & Sons Ltd, Chichester, England (2006)

[70] K. Rousseau, D. Dolphin, Tetrahedron Lett. 48 (1974) 4251-4254.

[71] P.A. Leermkers, H.T. Thomas, L.D. Weis, F.C. James, J. Am. Chem. Soc. 88 (1966) 5075-5083.

[72] A. Ron, M. Folman, O. Schnepp, J. Chem. Phys. 36 (1962) 2449.

[73] M.S.S. Hyung, L. Kevan, J. Chem. Soc., Faraday Trans. 94 (1998) 1417-1420.

[74] M.A.T. Marro, J.K. Thomas, J. Photochem. Photobiol., A 72 (1993) 251-259.

[75] H.M. SungSuh, Z.H. Luan, L. Kevan, J. Phys. Chem. B 101 (1997) 10455-10463.

[76] R.K.B. Bauer, R.; De Mayo, P.; Okada, K.; Rafalska, M.; Ware, W. R.; Wu, K. C., J. Am. Chem. Soc. 104 (1982) 4635-4644.

[77] I. Mochida, K. Tsuji, K. Suetsugu, H. Fujitsu, K. Takeshida, J. Phys. Chem. 84 (1980) 3159-3162.

[78] K. Kalyanasundaram, N. Vlachopoulos, V. Krishnan, A. Monnier, M. Gratzel, J. Phys. Chem. 91 (1987) 2342-2347.

[79] S. Nakagaki, C.R. Xavier, A.J. Wosniak, A.S. Mangrich, F. Wypych, M.P. Cantao, I. Denicolo, L.T. Kubota, Colloid Surf. A 168 (2000) 261-276.

[80] M.-C. Kuo, H.-F. Chen, J.-J. Shyue, D.M. Bassani, K.-T. Wong, Chem. Commun. 48 (2012) 8051-8053.

[81] T. Kobayashi, J-Aggregates, World Scientific Publishing Co. Pte. Ltd., Singapore (2012)

[82] Z. Chernia, D. Gill, Langmuir 15 (1999) 1625-1633.

[83] V.G. Kuykendall, J.K. Thomas, Langmuir 6 (1990) 1350-1356.

[84] A.K. Wertsching, A.S. Koch, S.G. DiMagno, J. Am. Chem. Soc. 123 (2001) 3932-3939.

[85] Y. Ishida, D. Masui, T. Shimada, H. Tachibana, H. Inoue, S. Takagi, J. Phys. Chem. C 116 7879-7885.

[86] S. Fiorilli, B. Onida, C. Barolo, G. Viscardi, D. Brunel, E. Garrone, Langmuir 23 (2007) 2261-2268.

Table 1 Amount of ZnP complexes loaded in the samples, as calculated by spectrophotometric and thermogravimetric analyses.

Samples	UV-Vis [a]		TGA [b]	
	% Weight	molecule/nm^2 [c]	% Weight	molecule/nm^2 [c]
ZnTBPP/SBA-	3.1	1/50	2.4	1/62

[a] Amount calculated by measuring the ZnP supernatant concentration before and after impregnation: for ZnTBPP in cyclohexane λ= 545; for ZnTPP in chloroform λ= 552 nm.

[b] Amount estimated on the basis of the measured weight loss between 100 and 800 °C.

[c] Values calculated by normalizing the measured weight % to the samples SSA reported in Table 2.

Table 2. Textural properties of the samples determined by nitrogen adsorption/desorption isotherms

Samples	SSA [a] ($m^2 \cdot g^{-1}$)	Pore diameter [b] (Å)	Total pore volume [c] ($cm^3 \cdot g^{-1}$)	Mesopore volume [d] ($cm^3 \cdot g^{-1}$)	Micropore volume [e] ($cm^3 \cdot g^{-1}$)
SBA-15	789	99	1.17	0.76	0.06
ZnTBPP/SBA-15	674	98	1.05	0.76	0.05
ZnTPP/SBA-15	625	98	0.97	0.72	0.05

[a] Calculated by the BET method. [b] Mean pore diameter calculated by the BJH method in the adsorption branch, employing the Kruk-Jaroniec-Sayari model. [c, d, e] Calculated by the BJH method: [c] in the 25-1000 Å, [d] in the 25-50 Å and [e] the 200-1000 Å ranges.

Table 3. Lifetime measurements of ZnP complexes in solution and immobilized in SBA-15 upon excitation at 455 nm.

Samples	τ_1	τ_2	$\chi^{2\,a}$
ZnTPP solution	40,0 ps	-	1,04
ZnTPP-SBA-15	45,0 ps	-	1,02
ZnTBPP solution	0,20 ns	-	1,10
ZnTBPP-SBA-15	0,54 ns	3,10 ns	1,09

[a] $\chi^2$is the correlation coefficient of the least squares fit of decay curves and is an indicator of the goodness of fit.

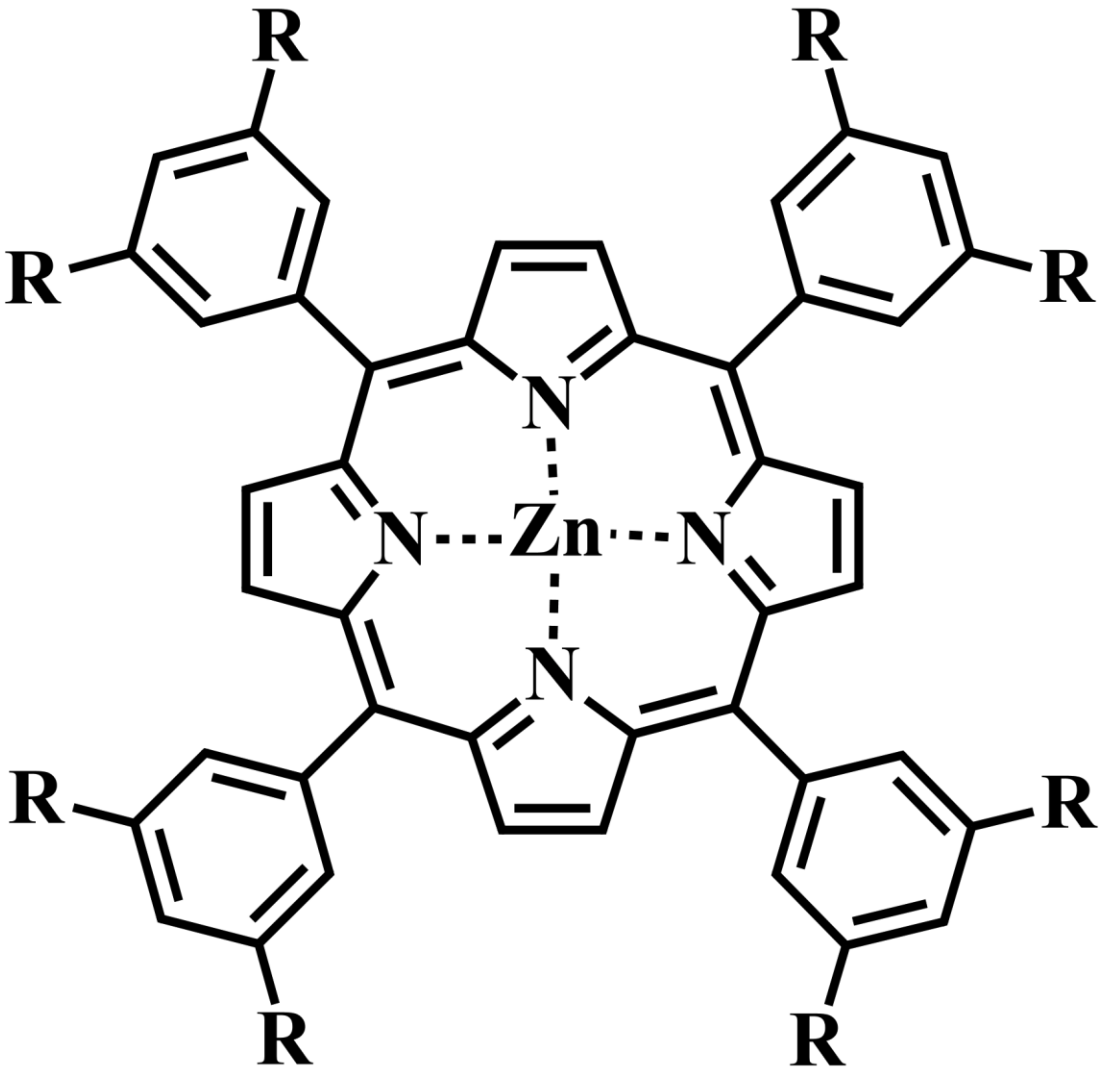

ZnTPP R = H

ZnTBPP R = *tert*-butyl

Scheme 1. Structure of Zn-5,10,15,20-tetrakis(3,5-di-tert-butylphenyl)porphyrin (ZnTBPP) and Zn-tetraphenylporphyrin (ZnTPP).

Figures captions

Figure 1. Effect of washing with the corresponding solvent (cyclohexane for ZnTBPP and chloroform for ZnTPP) on the ZnP/SBA-15 complexes as measured by spectrophotometric analysis. Values are referred to 1g of SBA-15.

Figure 2. XRD patterns of a) SBA-15, b) ZnTBPP/SBA-15 and c) ZnTPP/SBA- 15. Patterns were vertically shifted for easier comparison.

Figure 3. Adsorption (□) and desorption (×) isotherms of N_2 adsorbed at LNT on a) SBA-15, b) ZnTBPP/SBA-15 and c) ZnTPP/SBA- 15. Isotherms were vertically shifted for easier comparison.

Figure 4. FTIR spectra of ZnTBPP/SBA-15 (dotted), ZnTPP/SBA-15 (full line) and parent SBA-15 (dashed) in the high and low frequency ranges (top and bottom panels, respectively). For comparison the spectra measured on ZnTBPP and ZnTPP complexes diluted in KBr (vertically shifted for easier comparison) are reported in light grey and grey, respectively.

Figure 5. A) UV-Vis absorption and B) emission spectra of ZnTPP (red solid curve) and ZnTBPP (black dashed curve) in solution. Emission spectra were obtained upon excitation at 418 nm.

Figure 6 A) and B) UV-Vis absorption and C) emission spectra of ZnTPP/SBA-15 and corresponding solution (red solid and black dashed curves, respectively). D), E) and F) report the corresponding data for ZnTBPP/SBA-15. Emission spectra were obtained upon excitation at 418 nm. B) and E) insets are magnification of the adsorption spectra in the Q bands region.

Figure 1

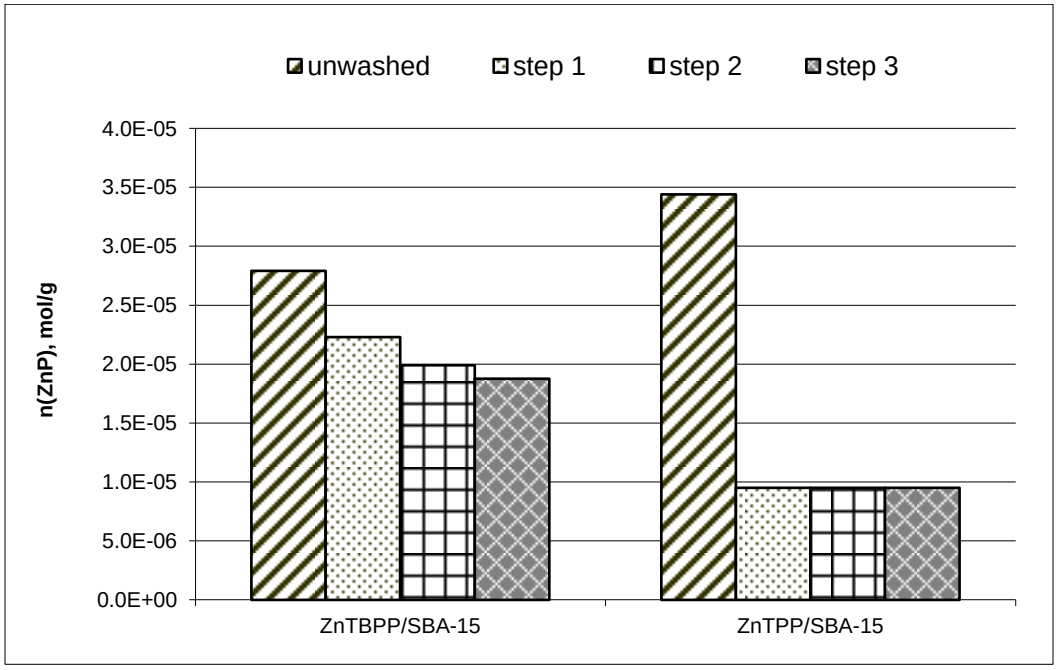
unwashed
step 1
step 2
step 3
4.0E-05
3.5E-05
3.0E-05
2.5E-05
2.0E-05
1.5E-05
1.0E-05
5.0E-06
0.0E+00
n(ZnP), mol/g
ZnTBPP/SBA-15
ZnTPP/SBA-15

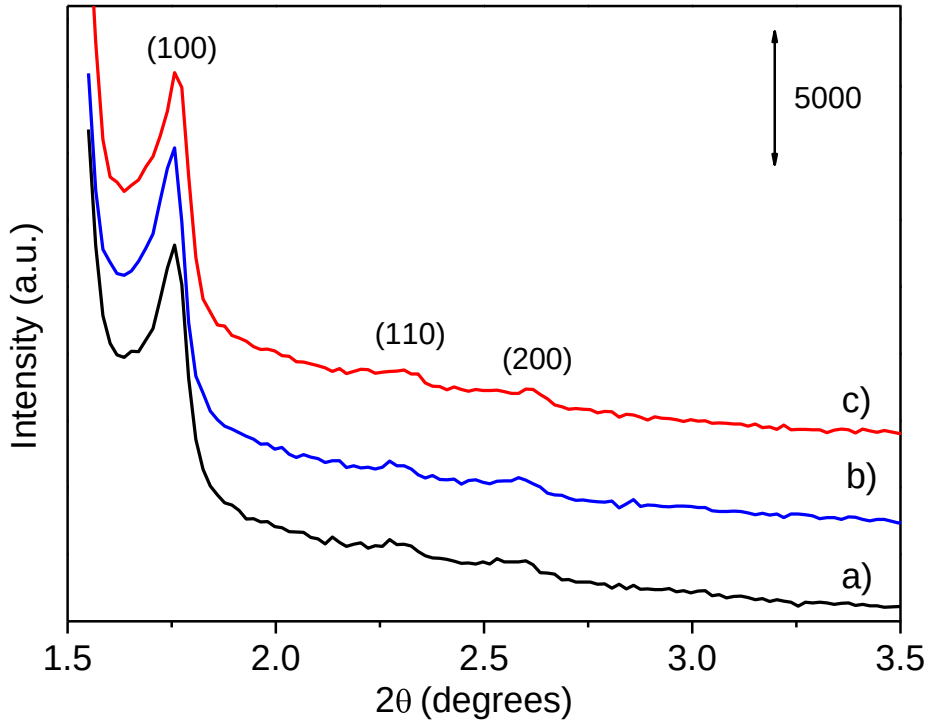

Figure 2

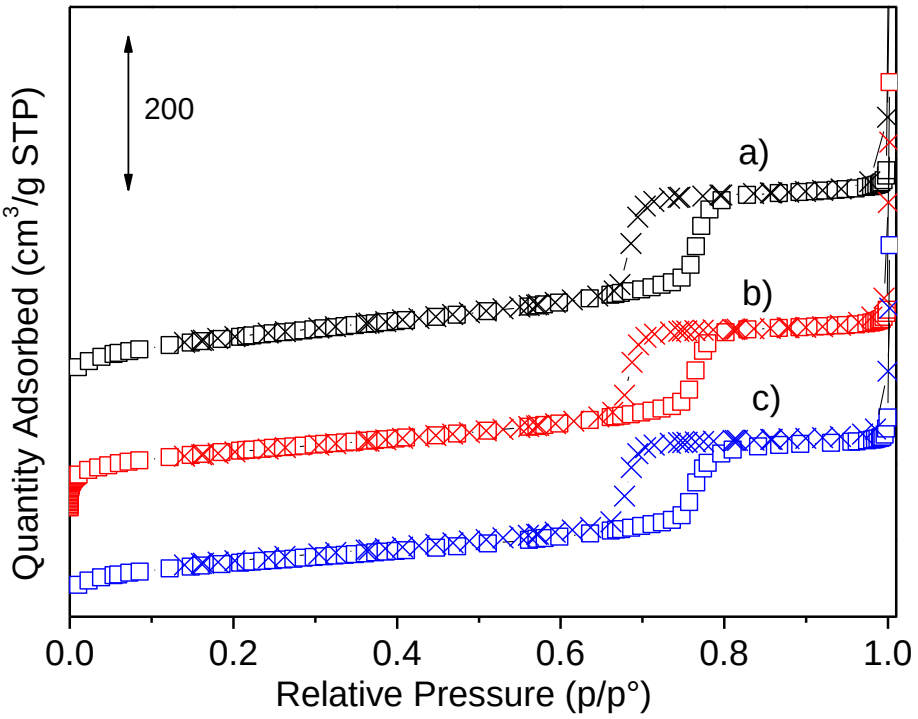
200
a)
b)
c)
Quantity Adsorbed (cm3/g STP)
0.0
0.2
0.4
0.6
0.8
1.0
Relative Pressure (p/p°)

Figure 3

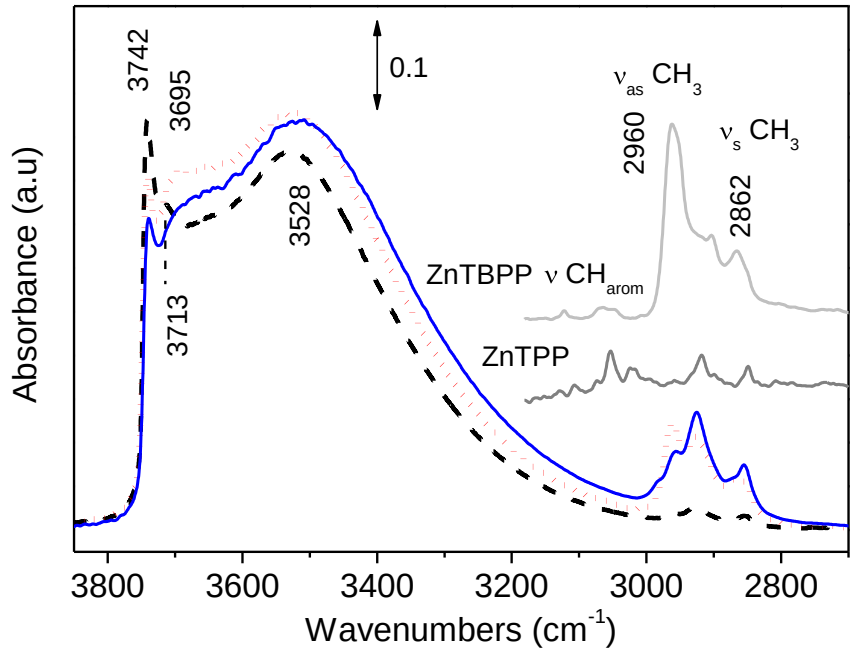
Absorbance (a.u)
0.1
3742
3695
3713
3528
ν_{as} CH_3
2960
ν_s CH_3
2862
ZnTBPP ν CH_{arom}
ZnTPP
3800
3600
3400
3200
3000
2800
Wavenumbers (cm^{-1})

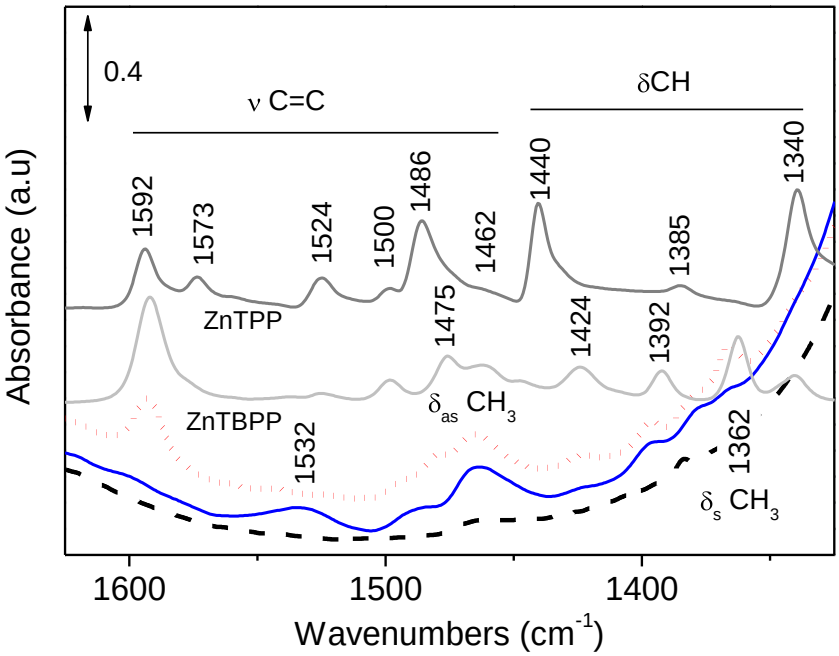
Absorbance (a.u)
0.4
ν C=C
δCH
1592
1573
1524
1500
1486
1462
1440
1385
1340
ZnTPP
1475
1424
1392
δ_{as} CH_3
ZnTBPP
1532
1362
δ_s CH_3
1600
1500
1400
Wavenumbers (cm^{-1})

Figure 4

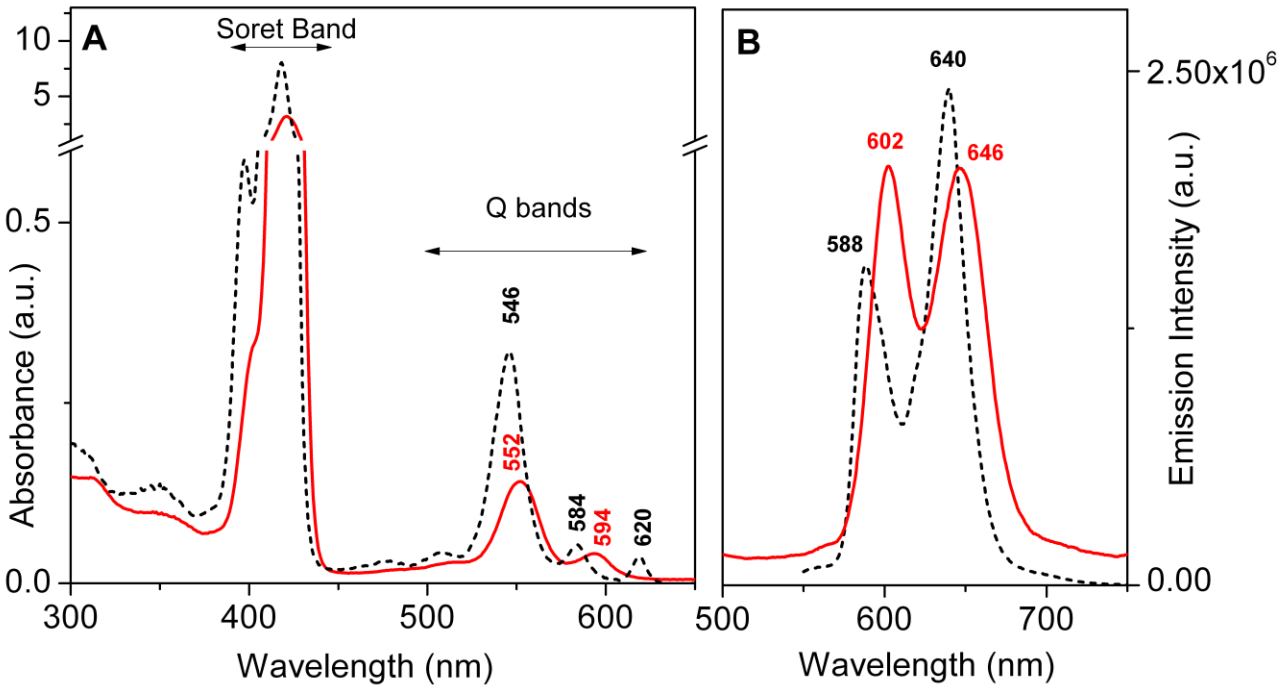
A
Soret Band
Q bands
546
552
584
594
620
Absorbance (a.u.)
Wavelength (nm)
B
640
602
646
588
Emission Intensity (a.u.)
2.50x10^6
0.00
Wavelength (nm)

Figure 5

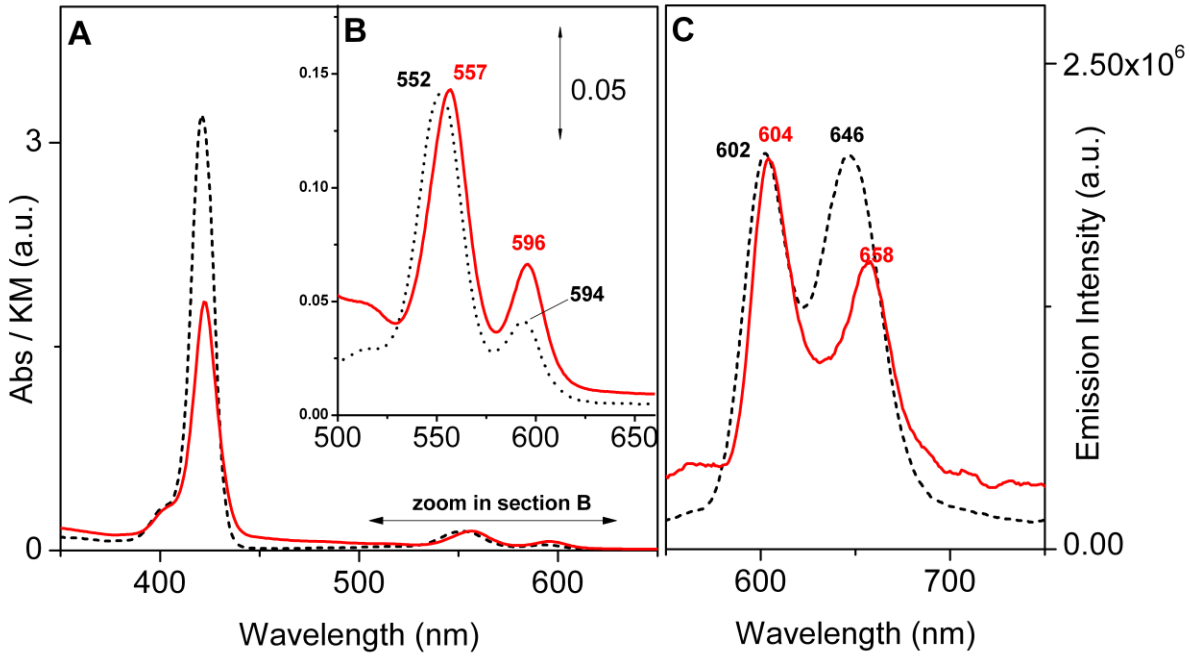
A
B
C
Abs / KM (a.u.)
3
0
400
500
600
Wavelength (nm)
552
557
596
594
0.05
0.15
0.10
0.05
0.00
500
550
600
650
zoom in section B
602
604
646
658
2.50x10^6
0.00
Emission Intensity (a.u.)
600
700
Wavelength (nm)

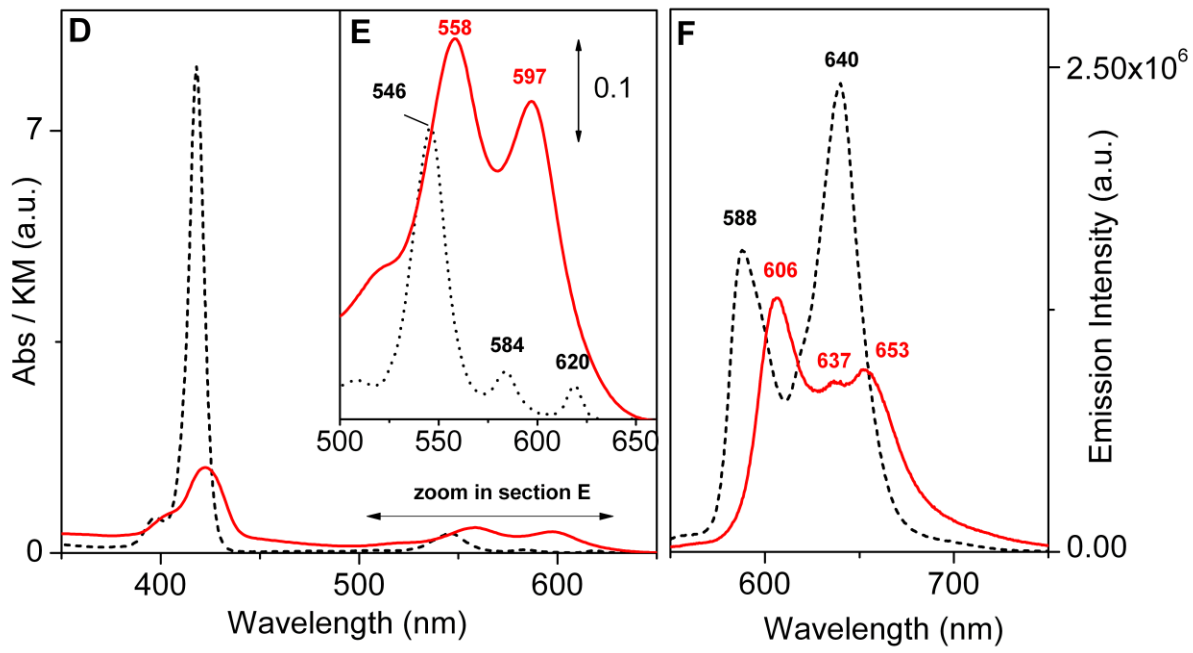
D
E
F
Abs / KM (a.u.)
Wavelength (nm)
Emission Intensity (a.u.)
2.50x10^6
0.00
558
546
597
0.1
584
620
zoom in section E
640
588
606
637
653

Figure 6